

The Shape of a Liquid Metal Jet under a Non-uniform Magnetic Field*

Shuzo OSHIMA**, Ryuichiro YAMANE,**
Yoshihiro MOCHIMARU** and Toshihiro MATSUOKA***

The shape of a horizontal slender jet of a liquid metal issuing from non-contacting circular nozzles under a non-uniform magnetic field is discussed. Our primary interests are to determine the shape of the free surface of the jet under such a field, and to demonstrate the possibility of the magnetic shape control of liquid metal jets. The basic equations of MHD flows are simplified by neglecting the terms concerning the viscosity, and solutions of the approximate analysis are presented. Parameters on which the magnetic shaping of jets are dependent are made clear. A jet with a circular initial shape forms a thin sheet, but maintains the same cross-sectional area. The shapes obtained by the approximate analysis are shown to be in good agreement with those of the experimental results using mercury.

Key Words: Fluid Mechanics, Magnetohydrodynamics, Liquid Metal Jet, Non-Uniform Magnetic Field, Metallurgy, Continuous Casting, Magnetic Shape-Control

1. Introduction

Much interest has arisen over the phenomena of liquid metal flow with a free surface under a magnetic field, in relation to the development and the design of atomic and metallurgical plants such as in the blanket cooling system of fusion power reactors, liquid metal MHD power systems, electromagnetic stirring devices, levitation melting devices, and others. In recent years, studies on the application of a levitation technique by using alternating magnetic fields for controlling the shape of liquid metal without contact have been actively conducted. For example, interesting results were given from the theoretical study of Shercliff⁽¹⁾ and the experimental investigations of Etay-Garnier⁽²⁾ and Garnier⁽³⁾.

In present metallurgical processes, contact between the molten metal and the walls is unavoidable, and the chemical and physical properties of the

products are degenerated by contamination arising from the walls. In present continuous casting plants, castings are limited in size due to the danger that the metal might solidify in the nozzle. Subsequent processes, such as rolling and forging, could perhaps be reduced and the quality of the solidified ingots or slabs be improved if a non-contacting shape control method were developed. Because the magnetic shape control method using alternating magnetic fields is based upon the skin effect, which causes the magnetic pressure, it requires relatively high-frequency alternating magnetic fields. Hence for the large deformation of a flowing molten metal surface a strong, high-frequency alternating magnetic field is required.

Formerly, we have made clear the effects of a magnetic field gradient on film flow by an approximate analysis and by experiments with mercury, and have demonstrated that the non-uniform magnetic field can act as a wall, without coming into contact with the fluid⁽⁴⁾⁽⁵⁾. In recent years, with the development of fusion power reactors, MHD power systems and the linear motor car, it has become relatively easy, from a technological viewpoint, to generate a strong, static magnetic field in a relatively large

* Received 16th, June, 1986. Paper No. 85-0981A, 85-0982A

** Tokyo Institute of Technology, Ookayama 2-12-1, Meguro-ku, Tokyo, 152, Japan

*** Japanese National Railway, Marunouchi 1-1, Chiyoda-ku, Tokyo, 100, Japan

space. We believe, therefore, that static magnetic fields are suitable for the non-contact shape control of flowing molten metals.

Many studies of a liquid jet without a magnetic field have been conducted since Rayleigh⁽⁶⁾ and Weber⁽⁷⁾. Many researchers have discussed its stability, the breakdown length and so on. Interesting and important results have been produced from the theoretical investigations of Taylor⁽⁸⁾, Clark⁽⁹⁾, Longuet-Higgins⁽¹⁰⁾, Tuch⁽¹¹⁾, Green⁽¹²⁾ and Geer⁽¹³⁾. However, the investigations of a liquid metal jet under a magnetic field are very rare. In this paper, we discuss the effect of non-uniform magnetic fields on a liquid metal jet, for the development of a non-contact shape control method using a magnetic field gradient.

2. Nomenclature

- a : nozzle radius
- B_0 : magnetic flux density vector in the non-uniform applied magnetic field zone
- B_{0u} : magnetic flux density vector in the uniform applied magnetic field zone ($B_{0u} = |B_{0u}|$)
- b_j : width of the jet
- b_n : nozzle width
- d : nozzle diameter = $2a$
- h_j : thickness of the jet
- h_n : nozzle height
- i_r, i_θ, j, k : unit vectors
- J : electric current density
- L : longitudinal characteristic length of the jet
- L_m : characteristic length of an applied magnetic field
- N_a : Stuart number
- p : pressure
- p_a : atmospheric pressure
- r, θ, z : cylindrical coordinates
- r_1, r_2 : principal curvatures of the jet surface
- r_p, r_{ps} : position vectors
- s : distance measured from the center
- v : velocity vector
- W_a : Weber number
- w_0 : main flow velocity
- x, y, z : coordinates
- $\varepsilon = a/L$
- $\varepsilon_m = a/L_m$
- ρ^* : non-dimensional coordinate = $r/s(\theta, z)$
- ρ_f : mass density
- σ : surface tension
- σ_e : electrical conductivity
- ϕ : electrostatic potential

3. Analysis

In this section, we analyze the shape of a horizontal slender jet of a liquid metal issuing from non-

conducting circular nozzles under a non-uniform magnetic field. We neglect the effects of gravity and viscosity, and assume that the initial velocity of the jet is uniform.

3.1 Basic equations

The basic equations of the steady flow of incompressible, conductive fluid under a magnetic field are written in the following vector forms.

$$(\mathbf{v} \cdot \nabla) \mathbf{v} = \frac{1}{\rho_f} \nabla p + \frac{1}{\rho_f} \mathbf{J} \times \mathbf{B}_0 \quad (1)$$

$$\mathbf{J} = \sigma_e (-\nabla \phi + \mathbf{v} \times \mathbf{B}_0) \quad (2)$$

$$\nabla \cdot \mathbf{v} = 0 \quad (3)$$

$$\nabla \cdot \mathbf{J} = 0 \quad (4)$$

$$\nabla \cdot \mathbf{B}_0 = 0 \quad (5)$$

$$\nabla \times \mathbf{B}_0 = 0 \quad (6)$$

In order to non-dimensionalize these vectors, the following variables are defined.

$$\left. \begin{aligned} \mathbf{v}^* &= \mathbf{v}/w_0, \quad p^* = p/\rho_f w_0^2 \\ \phi^* &= \phi/a w_0 B_{0u} \\ \mathbf{J}^* &= \mathbf{J}/\sigma_e w_0 B_{0u} \\ \nabla^* &= a \nabla, \quad \mathbf{B}_0^* = \mathbf{B}_0/B_{0u} \end{aligned} \right\} \quad (7)$$

Substituting the defined values of Eq. (7) into the vector forms, we have the following equations for the non-dimensional basic equations.

$$(\mathbf{v}^* \cdot \nabla^*) \mathbf{v}^* = -\nabla^* p^* + N_a (\mathbf{J}^* \times \mathbf{B}_0^*) \quad (8)$$

$$\mathbf{J}^* = -\nabla^* \phi^* + \mathbf{v}^* \times \mathbf{B}_0^* \quad (9)$$

$$\nabla^* \cdot \mathbf{v}^* = 0 \quad (10)$$

$$\nabla^* \cdot \mathbf{J}^* = 0 \quad (11)$$

$$\nabla^* \cdot \mathbf{B}_0^* = 0 \quad (12)$$

$$\nabla^* \times \mathbf{B}_0^* = 0 \quad (13)$$

where $N_a = \sigma_e B_{0u}^2 a / \rho_f w_0$ is the Stuart number of the jet.

3.2 Approximation for the basic equations

We express the non-dimensional velocity as follows

$$\mathbf{v}^* = \mathbf{v}_0^* + \mathbf{v}'^* \quad (14)$$

where \mathbf{v}_0^* is a uniform velocity and \mathbf{v}'^* is an additional velocity due to the shape change. When the shape of the jet is changed gradually, we can assume that $|\mathbf{v}'^*| \ll |\mathbf{v}_0^*|$. Substituting the above equation into Eqs. (8) and (9), and neglecting the small term, we obtain

$$(\mathbf{v}_0^* \cdot \nabla^*) \mathbf{v}'^* = -\nabla^* p^* + N_a (\mathbf{J}^* \times \mathbf{B}_0^*) \quad (15)$$

$$\mathbf{J}^* = -\nabla^* \phi^* + \mathbf{v}_0^* \times \mathbf{B}_0^* \quad (16)$$

From the above equations and Eqs. (10)~(14) we obtain the following differential equations:

$$\Delta^* p^* = -\frac{1}{2} N_a (\mathbf{v}_0^* \cdot \nabla^*) B_0^{*2} \quad (17)$$

$$\Delta^* \phi^* = 0 \quad (18)$$

where B_0^* indicates $|B_0^*|$. Since the distribution of the applied magnetic flux density B_0^* is a known function, Eq. (17) is a Poisson's equation. Under a uniform magnetic field, electric currents are not induced in an inviscid jet with a uniform velocity. Setting $\mathbf{J}^* = 0$ in

Eq.(16), we obtain

$$\nabla^* \phi_u^* = v_0^* \times B_0^* = C_1 \tag{19}$$

where C_1 is a constant vector. Resolving the above equation, we obtain

$$\phi_u^* = C_1 \cdot r_p^* + C_2 = (v_0^* \times B_0^*) \cdot r_p^* + C_2 \tag{20}$$

where C_2 and r_p^* are an arbitrary constant and a non-dimensional position vector, respectively. When the magnetic field strength changes very gradually, the above equations hold approximately, even in a non-uniform magnetic field. The non-dimensional electrostatic potential ϕ^* is given by

$$\left. \begin{aligned} \phi^* &= \phi_0^* + \phi'^* \\ \phi_0^* &= (v_0^* \times B_0^*) \cdot r_p^* \end{aligned} \right\} \tag{21}$$

where ϕ'^* is an additional electrostatic potential induced by the gradient of the applied magnetic field. We assume that $|\phi'^*| \ll |\phi_0^*|$.

Here, we choose the co-ordinate system as follows :

$$\left. \begin{aligned} z^* &= z/L, r^* = r/a \\ \theta^* &= \theta \end{aligned} \right\} \tag{22}$$

where L is a characteristic length (see Fig. 1). Also, B_0^* and v_0^* are given by

$$\left. \begin{aligned} B_0^* &= B^*(z^*)j \\ v_0^* &= k \end{aligned} \right\} \tag{23}$$

where j and k are unit vectors in the direction of the y - and z - axes, respectively. Substituting Eqs.(21) ~ (23) into Eq.(18), we obtain

$$\begin{aligned} \frac{1}{r^*} \frac{\partial}{\partial r^*} \left(r^* \frac{\partial \phi'^*}{\partial r^*} \right) + \frac{1}{r^{*2}} \frac{\partial^2 \phi'^*}{\partial \theta^{*2}} + \epsilon^2 \frac{\partial^2 \phi'^*}{\partial z^{*2}} \\ + \epsilon^2 \frac{\partial^2 \phi_0^*}{\partial z^{*2}} = 0 \end{aligned} \tag{24}$$

where $\epsilon = a/L$, and we assume that $\epsilon \ll 1$. We consider ϕ'^* in an asymptotic expansion in ϵ^2 as follows

$$\phi'^* = \epsilon^2 \phi_1^* + \epsilon^4 \phi_2^* + \dots + (\epsilon^2)^n \phi_n^* + \dots \tag{25}$$

The leading term of ϕ^* is ϕ_0^* of Eq.(21). Substituting the above equation into Eq.(24) and collecting the same order terms, we obtain

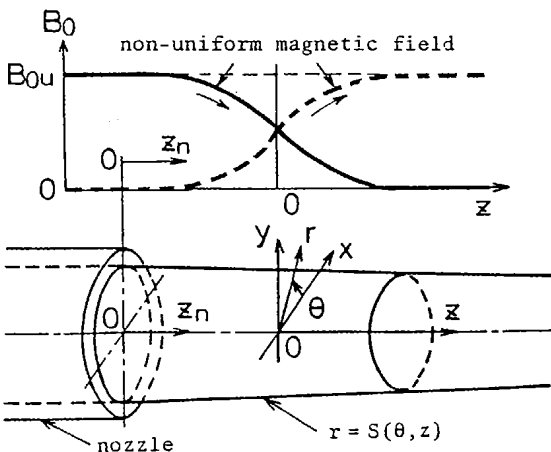


Fig. 1 Coordinate system

$$\begin{aligned} \frac{1}{r^*} \frac{\partial}{\partial r^*} \left(r^* \frac{\partial r_{n+1}^*}{\partial \theta^{*2}} \right) + \frac{1}{r^{*2}} \frac{\partial \phi_{n+1}^*}{\partial \theta^{*2}} \\ = - \frac{\partial^2 \phi_n^*}{\partial z^{*2}} \quad (n \geq 0) \end{aligned} \tag{26}$$

On the other hand, substituting Eq.(23) into Eq.(17), we obtain the following equation for the non-dimensional pressure p^* .

$$\begin{aligned} \frac{1}{r^*} \frac{\partial}{\partial r^*} \left(r^* \frac{\partial p^*}{\partial r^*} \right) + \frac{1}{r^{*2}} \frac{\partial^2 p^*}{\partial \theta^{*2}} + \epsilon^2 \frac{\partial^2 p^*}{\partial z^{*2}} \\ = - \frac{1}{2} \epsilon N_a G^*(z^*) \end{aligned} \tag{27}$$

where $G^*(z^*) = dB^{*2}(z^*)/dz^*$. We neglect the third term on the left-hand side of the above equation as a small, higher order term.

$$\frac{1}{r^*} \frac{\partial}{\partial r^*} \left(r^* \frac{\partial p^*}{\partial r^*} \right) + \frac{1}{r^{*2}} \frac{\partial^2 p^*}{\partial \theta^{*2}} = - \frac{1}{2} \epsilon N_a G^*(z^*) \tag{28}$$

The right-hand side term of the above equation is a known function. Once the boundary conditions are given in the (r^*, θ^*) -plane, pressures everywhere in the jet is determined by solving the above equation.

Now, we estimate the order of each term of the equation of motion. We denote the right-hand side terms of Eq.(15) by F^* . Then,

$$F^* = F_p^* + F_m^* = -\nabla^* p^* + N_a (J \times B_0^*) \tag{29}$$

where F_p^* and F_m^* are pressure and electromagnetic force terms, respectively. Using Eqs.(16), (21) and (25), each component of the non-dimensional current density vector J^* is given by

$$\left. \begin{aligned} J_r^* &= -\epsilon^2 \frac{\partial \phi_1^*}{\partial r^*} + O(\epsilon^4) \\ J_\theta^* &= -\frac{\epsilon^2}{r^*} \frac{\partial \phi_1^*}{\partial \theta^*} + O(\epsilon^4) \\ J_z^* &= \epsilon \frac{\partial \phi_0^*}{\partial z^*} + O(\epsilon^3) \end{aligned} \right\} \tag{30}$$

Thus, each component of F_p^* and F_m^* has the following orders

$$\left. \begin{aligned} F_{pr}^* \sim O(1), F_{p\theta}^* \sim O(1), F_{pz}^* \sim O(\epsilon) \\ F_{mr}^* \sim O(\epsilon N_a), F_{m\theta}^* \sim O(\epsilon N_a), F_{mz}^* \sim O(\epsilon^2 N_a) \end{aligned} \right\} \tag{31}$$

Assuming that $\epsilon \ll 1$, we find from the above that the longitudinal force acting on the jet is smaller than the cross-sectional one and that the change in area is smaller than the change in shape. Thus, we may consider that

$$|v_r^*|, |v_\theta^*| \gg |v_z^*| \tag{32}$$

Substituting Eqs.(16) (21), (25) and (30) into Eq.(15), we obtain the following differential equations for v_r^* and v_θ^* .

$$\epsilon \frac{\partial v_r^*}{\partial z^*} = - \frac{\partial}{\partial r^*} \left[p^* + \frac{1}{4} \epsilon N_a r^{*2} G^*(z^*) \cos^2 \theta^* \right] \tag{33}$$

$$\begin{aligned} \epsilon \frac{\partial v_\theta^*}{\partial z^*} = - \frac{1}{r^*} \frac{\partial}{\partial \theta^*} \left[p^* + \frac{1}{4} \epsilon N_a r^{*2} G^*(z^*) \right. \\ \left. \times \cos^2 \theta^* \right] \end{aligned} \tag{34}$$

In resolving these equations, we have to know the boundary conditions on the free surface of the jet and the upstream conditions.

3.3 Boundary conditions

In this section we formulize the boundary conditions. Let the position vector r_{ps} , which denotes the position of the free surface of the jet, be

$$r_{ps}(\theta, z) = z\mathbf{k} + s(\theta, z)\mathbf{i}_r \tag{35}$$

From the above equation, e_θ and e_x , which are unit vectors on the boundary surface, are given by

$$e_\theta = \frac{\partial \mathbf{r}}{\partial \theta} = \frac{\partial s}{\partial \theta} \mathbf{i}_r + s \frac{\partial \mathbf{i}_r}{\partial \theta} = s_\theta \mathbf{i}_r + s \mathbf{i}_\theta \tag{36}$$

$$e_z = \frac{\partial \mathbf{r}}{\partial z} = \mathbf{k} + \frac{\partial s}{\partial z} \mathbf{i}_r = \mathbf{k} + s_z \mathbf{i}_r \tag{37}$$

where the subscripts of s denote differentiation with respect to these vectors. From these equations, the normal vector e_n is given by

$$e_n = e_\theta \times e_z = s \mathbf{i}_r - s \mathbf{i}_\theta - s s_z \mathbf{k} \tag{38}$$

The velocity vector u is approximately given by

$$v = v'_r \mathbf{i}_r + v'_\theta \mathbf{i}_\theta + w_0 \mathbf{k} \tag{39}$$

Using Eqs.(38) and (39), the condition that the fluid must flow along its own free surface is expressed as follows

$$e_n \cdot v = s v'_r - s_\theta v'_\theta - s s_z w_0 = 0 \tag{40}$$

Denoting the above equation with non-dimensional variables, we obtain

$$\varepsilon s^* s'^*_{z^*} = s^* v'_{r^*} - s^* s'^*_{\theta^*} v'_{\theta^*} \tag{41}$$

We now induce the boundary condition for the pressure. At the free surface, the jump in pressure δp due to surface tension is given by

$$\delta p = p - p_a = \sigma \left(\frac{1}{r_1} + \frac{1}{r_2} \right) \tag{42}$$

where $1/r_1 + 1/r_2$ is twice the mean curvature of the surface, and p_a is the pressure of the surrounding atmosphere. When the position of the surface is denoted as in Eq.(35), we obtain the following equation

$$\frac{1}{r_1} + \frac{1}{r_2} = - \{s^2(1+s_z^2) + s_\theta^2\}^{-3/2} \cdot \{s s_{zz}(s^2 + s_\theta^2) - 2(ss_{\theta z} - s_z s_\theta) s_z s_\theta + (1+s_z^2)(s s_{\theta\theta} - 2s s'_\theta - s^2)\} \tag{43}$$

Using non-dimensional variables, we find that Eq.(43) can be written as follows.

$$\frac{1}{r_1^*} + \frac{1}{r_2^*} = \frac{s^{*2} + 2s^*_{\theta^*}{}^2 - s^* s^*_{\theta^*}{}^2}{(s^{*2} + s^*_{\theta^*}{}^2)^{3/2}} + O(\varepsilon^2) \tag{44}$$

Substituting Eq.(44) into Eq.(42), we obtain

$$p^* = \frac{1}{W_a} \frac{s^{*2} + 2s^*_{\theta^*}{}^2 - s^* s^*_{\theta^*}{}^2}{(s^{*2} + s^*_{\theta^*}{}^2)^{3/2}} \tag{45}$$

where $W_a = \rho_f a w_0^2 / \sigma$ is the Weber number of the jet, based on the nozzle radius. Thus, Eqs.(41) and (45) are the boundary conditions for the fluctuating velocity component v'^* and for the pressure p^* , respectively.

4. Analytical solutions

We make the following variable conversion for p^*

and s^* .

$$p^* = -\frac{1}{8} \varepsilon N_a G^*(z^*) (r^{*2} - 1) + \frac{1}{w_a} + \phi^* \tag{46}$$

$$s^*(\theta^*, z^*) = 1 + s'^*(\theta^*, z^*) \tag{47}$$

where s'^* is the fluctuating component of the free surface. When the shape change of the jet is small, we can assume that $|s'^*| \ll 1$. We then introduce the change of the independent variable as follows.

$$\left. \begin{aligned} (r^*, \theta^*, z^*) &\rightarrow (\rho^*, \theta^*, z^*) \\ \rho^* &= \frac{r^*}{s^*(\theta^*, z^*)} \end{aligned} \right\} \tag{48}$$

Thus, r is stretched in a non-uniform manner, but the unknown boundary $r^* = s^*(\theta^*, z^*)$ is mapped onto the known boundary $\rho^* = 1$. Using the independent variables ρ^*, θ^* and z^* and the dependent variables $\phi^*(\rho^*, \theta^*, z^*)$, $v'^*(\rho^*, \theta^*, z^*)$ and $s'^*(\rho^*, \theta^*, z^*)$, Eqs.(28), (33), (41) and (45) can be written as

$$\frac{1}{\rho^*} \frac{\partial}{\partial \rho^*} \left(\rho^* \frac{\partial \phi^*}{\partial \rho^*} \right) + \frac{1}{\rho^{*2}} \frac{\partial^2 \phi^*}{\partial \theta^{*2}} = 0 \tag{49}$$

$$\varepsilon \frac{\partial v'^*_{r^*}}{\partial z^*} = -\frac{\partial}{\partial \rho^*} \left[\phi^* + \frac{1}{8} \varepsilon N_a \rho^{*2} G^*(z^*) \cos 2\theta^* \right] \tag{50}$$

$$\varepsilon \frac{\partial s'^*}{\partial z^*} = v'^*_{r^*} \quad (\rho^* = 1) \tag{51}$$

$$\phi^* = -\frac{1}{W_a} (s'^* + s'^*_{\theta^*}) + \frac{1}{4} \varepsilon N_a G^*(z^*) s'^* \quad (\rho^* = 1) \tag{52}$$

Here, we consider the following series for the solution.

$$\begin{aligned} \phi^* &= f^*_{\phi 1}(\rho^*) g^*_{\phi 1}(z^*) \cos \theta^* + f^*_{\phi 2}(\rho^*) g^*_{\phi 2}(z^*) \\ &\times \cos 2\theta^* + \dots + f^*_{\phi n}(\rho^*) g^*_{\phi n}(z^*) \cos n\theta^* \\ &+ \dots \end{aligned} \tag{53}$$

$$\begin{aligned} v'^*_{r^*} &= f^*_{v 1}(\rho^*) g^*_{v 1}(z^*) \cos \theta^* + f^*_{v 2}(\rho^*) g^*_{v 2}(z^*) \\ &\times \cos 2\theta^* + \dots + f^*_{v n}(\rho^*) g^*_{v n}(z^*) \cos n\theta^* \\ &+ \dots \end{aligned} \tag{54}$$

$$\begin{aligned} s'^* &= g^*_{s 1}(z^*) \cos \theta^* + g^*_{s 2}(z^*) \cos 2\theta^* + \dots \\ &+ g^*_{s n}(z^*) \cos n\theta^* + \dots \end{aligned} \tag{55}$$

Substituting Eq.(53) into Eq.(49), we obtain

$$\frac{1}{\rho^*} \frac{d}{d\rho^*} \left(\rho^* \frac{df^*_{\phi n}}{d\rho^*} \right) - \frac{n^2}{\rho^{*2}} f^*_{\phi n} = 0 \quad (n \geq 1) \tag{56}$$

Since $f^*_{\phi n}$ is finite at the center of the jet ($\rho^* = 0$), we find the following solution for Eq. (56).

$$f^*_{\phi n} = A_n \rho^{*n} \tag{57}$$

Substituting Eqs.(53)~(55) into Eqs.(50)~(52), we obtain

$$\begin{aligned} A_n g^*_{\phi n}(z^*) &= \left\{ \frac{1}{W_a} (n^2 - 1) + \frac{1}{4} \varepsilon N_a G^*(z^*) \right\} \\ &\times g^*_{s n}(z^*) \quad (n \geq 1) \end{aligned} \tag{58}$$

$$\begin{aligned} \varepsilon f^*_{v n}(\rho^*) \frac{dg^*_{v n}(z^*)}{dz^*} &= -n A_n \rho^* g^*_{\phi n}(z^*) \\ &- \frac{1}{4} \varepsilon N_a \delta_{2n} \times \rho^* G^*(z^*) \end{aligned} \tag{59}$$

$$\varepsilon \frac{dg^*_{s n}(z^*)}{dz^*} = f^*_{v n}(1) g^*_{v n}(z^*) \tag{60}$$

where δ_{ij} denotes Kronecker's symbol. The above equations give us the following equation for $g^*_{s n}(z^*)$.

$$\begin{aligned} \epsilon^2 \frac{d^2 g_{sn}^*(z^*)}{dz^{*2}} = & -\frac{1}{W_a} n(n^2-1)g_{sn}^*(z^*) \\ & -\frac{1}{4}\epsilon N_a \{ \delta_{2n} + n g_{sn}^*(z^*) \} \cdot G(z^*) \end{aligned} \quad (61)$$

The first term on the right-hand side of Eq.(61) is due to the surface tension, and the second term is due to the electromagnetic force. In the case without a magnetic field ($N_a=0$) we have the following oscillatory solution for $g_{sn}^*(z^*)$.

$$g_{sn}^*(z^*) = D_n R e^{i(\omega_n^* z^* + \varphi_n)} \quad (62)$$

where D_n and φ_n are arbitrary constants, and ω_n^* is a non-dimensional angular frequency given by the following equation.

$$\omega_n^* = \sqrt{\frac{n(n^2-1)}{\epsilon^2 W_a}} \quad (63)$$

The wavelength of the n -th mode deformation, λ_n , is given by

$$\lambda_n = 2\pi a \sqrt{\frac{W_a}{n(n^2-1)}} \quad (64)$$

This equation is consistent with that of Rayleigh⁽⁶⁾. A jet with an n -th mode shape change oscillates in wave length λ_n . If the surface of the deformed jet is relatively smooth, we may consider that the derivative of s^* with respect to θ is small.

$$|n g_{sn}^*(z^*)| \ll 1 \quad (65)$$

In such a case, we can easily find, by Eq.(61), that the second mode ($n=2$) of the shape change becomes predominant. This is understandable in view of the fact that the shape change of the jet is due to the eddycurrent. In the right half of the jet, the current flow is in one direction, while in the left half, the current direction is the opposite. Thus, the jet is narrowed or widened by the electromagnetic force which is induced by the interaction of the eddycurrent and the applied magnetic field. The changed shape is symmetric with respect to the y - as well as the x - axis. This condition is well satisfied by the function $\cos 2\theta^*$. Therefore, we consider the second mode of shape change only. Equation (61) gives the following equation for the shape change by the electromagnetic force.

$$\epsilon^2 \frac{d^2 g_{s2}^*(z^*)}{dz^{*2}} = -\frac{6}{W_a} g_{s2}^*(z^*) - \frac{1}{4}\epsilon N_a G^*(z^*) \quad (66)$$

Now, we consider a non-uniform applied magnetic field, such that (see Fig.2)

$$B_0^{*2} = \frac{1}{2} \left(1 - \tanh \frac{L}{L_m} z^* \right) \quad (67)$$

where L_m is a characteristic length of the non-uniform magnetic field zone. Substituting the above equation into the second term on the right-hand side of Eq. (66), we obtain

$$\left(\frac{d^2}{dz^{*2}} + \frac{6}{W_a} \right) g_{s2}^*(z^*) = -\frac{\epsilon_m N_a}{8} \frac{1}{\cosh^2(\epsilon_m z^*)} \quad (68)$$

where $\epsilon_m = a/L_m$ and $z^* = z/\epsilon$. Resolving the above equation under the condition that $g_{s2} = dg_{s2}/dz^* = 0$ for

the limit ($z^* \rightarrow -\infty$), we obtain the following solution for $g_{s2}(z^*)$.

$$\begin{aligned} g_{s2}^*(z^*) = & \beta \sin(\alpha z^*) \int_{-\infty}^{z^*} \frac{\cos(at)}{\cosh^2(\epsilon_m t)} dt \\ & - \beta \cos(\alpha z^*) \int_{-\infty}^{z^*} \frac{\cos(at)}{\cosh^2(\epsilon_m t)} dt \end{aligned} \quad (69)$$

where $\alpha = \sqrt{6/W_a}$ and $\beta = \epsilon_m N_a / 8\alpha$. When the effect of the surface tension is small, we can neglect the second term on the left-hand side. In such a case, we obtain the following solution for $g_{s2}(z^*)$.

$$g_{s2}^*(z^*) = \frac{N_a}{8} \left\{ z^* + \frac{1}{\epsilon_m} \log(e^{\epsilon_m z^*} + e^{-\epsilon_m z^*}) \right\} \quad (70)$$

In the region that $z^* \gg 1$, the above equation is satisfactorily approximated by the following equation.

$$g_{s2}^*(z^*) = N_a z^* / 4 \quad (71)$$

Thus, in the case of a small and smooth change, the free surface of the liquid metal issuing from the circular nozzle changes in shape in the mode of $\cos 2\theta^*$. The deformation rate of the jet shape is proportional to the Stuart number N_a . When the applied magnetic field is given by Eq.(72), we obtain the following solutions for $g_{s2}^*(z^*)$ as Eqs. (73)~(75).

$$B_0^{*2}(z^*) = \frac{1}{2} (1 + \tanh \epsilon_m z^*) \quad (72)$$

$$\begin{aligned} g_{s2}^*(z^*) = & -\beta \sin(\alpha z^*) \int_{-\infty}^{z^*} \frac{\cos(at)}{\cosh^2(\epsilon_m t)} dt \\ & + \beta \cos(\alpha z^*) \int_{-\infty}^{z^*} \frac{\sin(at)}{\cosh^2(\epsilon_m t)} dt \end{aligned} \quad (73)$$

$$g_{s2}^*(z^*) = \frac{N_a}{8} \left\{ z^* + \frac{1}{\epsilon_m} \log(e^{\epsilon_m z^*} + e^{-\epsilon_m z^*}) \right\} \quad (74)$$

$$g_{s2}^*(z^*) = -N_a z^* / 4 \quad (75)$$

When the gradient of the applied magnetic field changes in sign, the shape change due to the electromagnetic force also changes.

5. Analytical results

Solutions for $g_{s2}^*(z^*)$ are governed by three non-dimensional parameters N_a, W_a and ϵ_m . The Stuart number N_a is a non-dimensional parameter that denotes the ratio of the electromagnetic force to the

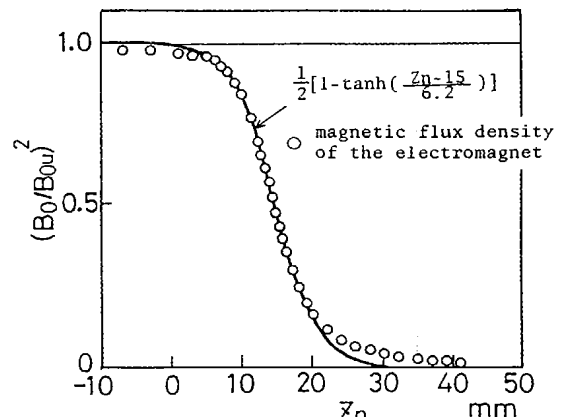


Fig. 2 Distribution of the applied magnetic field

inertial force. The Weber number W_a is the ratio of the dynamic pressure to the pressure rise by surface tension. The parameter ϵ_m is the ratio of the nozzle radius a to the characteristic length of the non-uniform magnetic field zone L_m . It denotes the approximate ratio of the longitudinal length of the eddy-current to its width. We now present the analytical results for the case of a non-uniform magnetic field which decreases in the streamwise direction.

At first, we examine the effect of the Stuart number N_a on the shape change of the jet. We calculate the shape for various Stuart numbers from 0.1 to 0.5, keeping W_a and ϵ_m constant. The distribution of the width of the jet is shown in Fig.3. The jet is widened by the electromagnetic force, and the width of the jet increases with increasing N_a .

Next, we calculate the shape for various Weber numbers to examine the effect of surface tension, keeping the other parameters constant (see Fig.4). The width of the jet increases with an increase in the Weber number W_a . Except for the case where $W_a = \infty$, the widened jet width is restored to its initial value under the influence of the surface tension, and then it oscillates widthwise in the streamwise direction. The wavelength of this oscillation increases with an increasing W_a .

Finally, we calculate the shape for various ϵ_m to examine the effect of the distribution of the applied magnetic flux density on the shape change, keeping $N_a = 0.2$ and $W_a = 400$ (see Fig.5). In the upstream region,

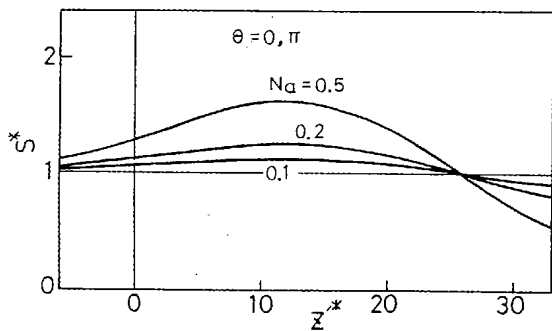


Fig. 3 Dependence on the Stuart number N_a

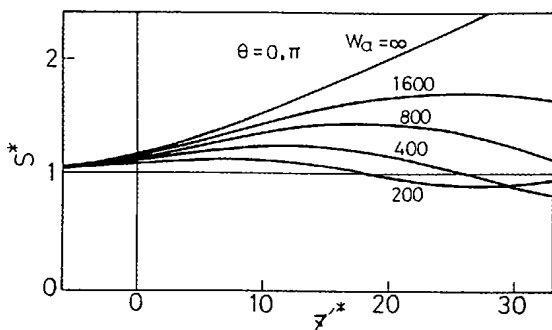


Fig. 4 Dependence on the Weber number W_a

where the shape change is relatively small, the shape change for a small ϵ_m is larger than that for a large ϵ_m . In the downstream region, however, the shape change for a small ϵ_m is smaller than that for a large ϵ_m . The electromagnetic force induced for a small ϵ_m , acting on the fluid through the wide region, however, is weaker than that for a large ϵ_m . Thus, in the case of small ϵ_m , the jet shape changes gradually under the influence of not only the electromagnetic force but also of the surface tension.

6. Experiments

6.1 Experimental apparatus and procedure

The experimental apparatus, shown diagrammatically in Fig.6, consists of a nozzle, an electromagnet and feeding cycles. In this system, mercury is fed to the channel by a difference in height between the upper reservoir and the nozzle. The tip of the electromagnetic pole is rectangular in shape, 350mm long and 160mm wide, and the gap between the poles is 50mm. The nozzle exit is located 13mm inside the edge of the poles so that the fluid will flow under a non-uniform magnetic field zone. The working fluid accumulated in a lower reservoir is returned to the upper reservoir continuously by a mercury pump. In order to maintain

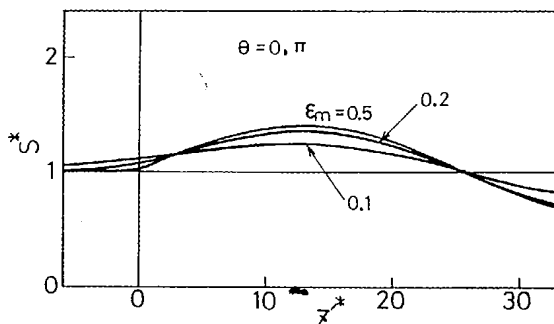


Fig. 5 Dependence on the non-dimensional parameter ϵ_m

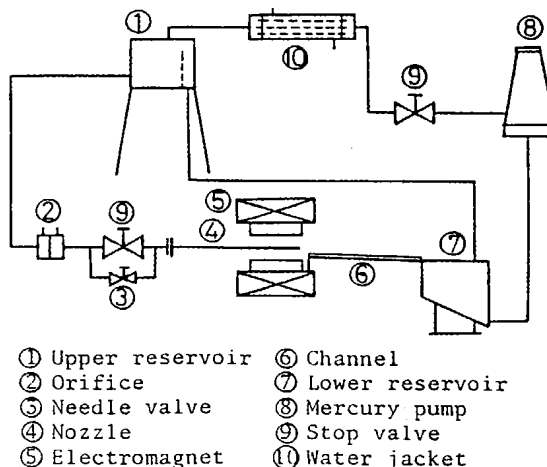
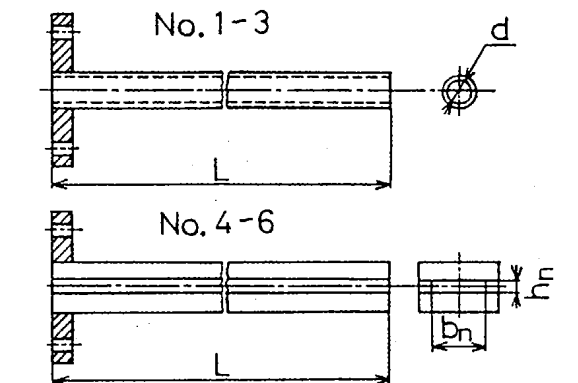


Fig. 6 Schematic diagram of the experimental apparatus

the fluid at a constant temperature, a water jacket is attached to the mercury loop. The flow rate is adjusted with a needle valve and measured by a pipe orifice. The magnetic flux density of the electromagnet can be changed continuously up to 1.48T by regulating the amperage of the current. In this experiment, we attached steel sheets between the poles to change the length of the non-uniform magnetic field zone. We used several types of nozzles as shown in Table 1. The shape of the jet is measured by a spot electrode probe which is shown in Fig.7. The measuring apparatus consists of four spot electrode probes, and it is attached to a reading microscope. The position of the probe is changed and measured three-dimensionally. The electrodes of the probe are made of 0.2 mm diameter stainless wire and the tips are filed and sharpened. The probe is electrically connected through a D.C. power supply to an anode, which is attached to the upper reservoir, and the circuit is closed through the fluid. As the jet contains the small disturbance on its surface, an electric circuit must be constructed to obtain the time-averaged position of the surface. The electric circuit, shown in Fig.7, contains two LED's (Luminous Electric Diode) and an ammeter. Both of them emit light, depending on whether or not the probe contacts the surface. If both LED's turn on and off with the same brightness, then the intermittency factor of the surface can be judged to be about 0.5 and the position of the probe can be measured. When the probe perfectly contacts the fluid, an electric current of 0.5mA flows through the fluid.

Table 1 Dimensions and materials of the nozzle



Nozzle type	No.	Dimensions(mm)		Material
		d	L	
Circular pipe	1	6	700	Glass
	2	8	700	
	3	10	700	
Rectangular pipe	4	$h_n \times b_n$	L	Acrylate resin
	5	2 x 10	700	
	6	3 x 15	700	

We may consider that the effect of this current on the jet is negligibly small.

The coordinate system we used is shown in Fig.7. As the jet issuing from the horizontal nozzle droops under the influence of gravity, the shape obtained by the probe is different from the real cross-sectional shape which is perpendicular to the flow. We obtained the shape perpendicular to the flow by the following procedure. At first, we obtained the barycenter of the shape which is measured perpendicularly to the z axis. Then, we obtained the barycenter curve in the y-z plane by connecting the neighboring barycenters with a curve. Next, we calculated the gradient of the barycenter curve and obtained the values of cosine at all points where the jet shape was measured. Finally, we obtained the cross-sectional shape by correcting the measured shape with the cosine values.

6.2 Experimental results

We examine the effects of the applied magnetic field strength and the shape of the nozzle.

6.2.1 Dependence on the applied magnetic field strength

At first, we examine the dependence of the shape change on the applied magnetic field strength. We used a nozzle of 8mm inside diameter and changed the applied magnetic flux density from 0 to 2.02 T, keeping the exit mean velocity w_o at 2.10m/s. The Stuart

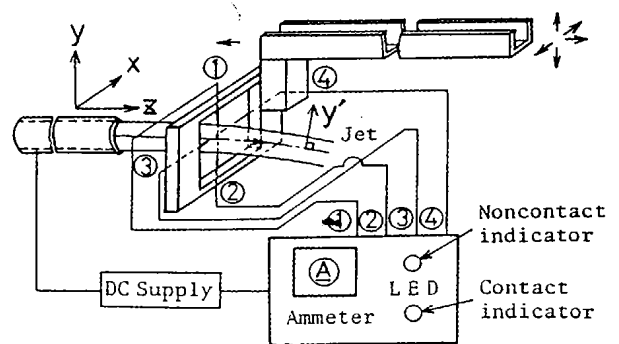


Fig. 7 Diagram of the measuring equipment

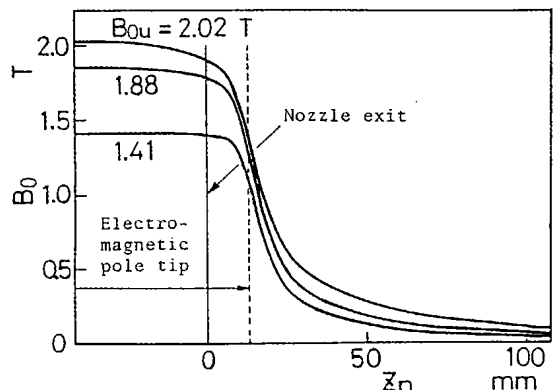


Fig. 8 Distribution of the applied magnetic flux density

number N_a increased with increasing applied magnetic field strength. The distribution of the magnetic flux density measured by a Gauss meter is shown in Fig.8. The origin of the z_n - axis is located at the nozzle

exit. Photographs of the jet and the cross sectional shape, measured by a spot electrode probe, are shown in Figs.9 and 10, respectively. The jet is widened by the electromagnetic force and the width of the jet

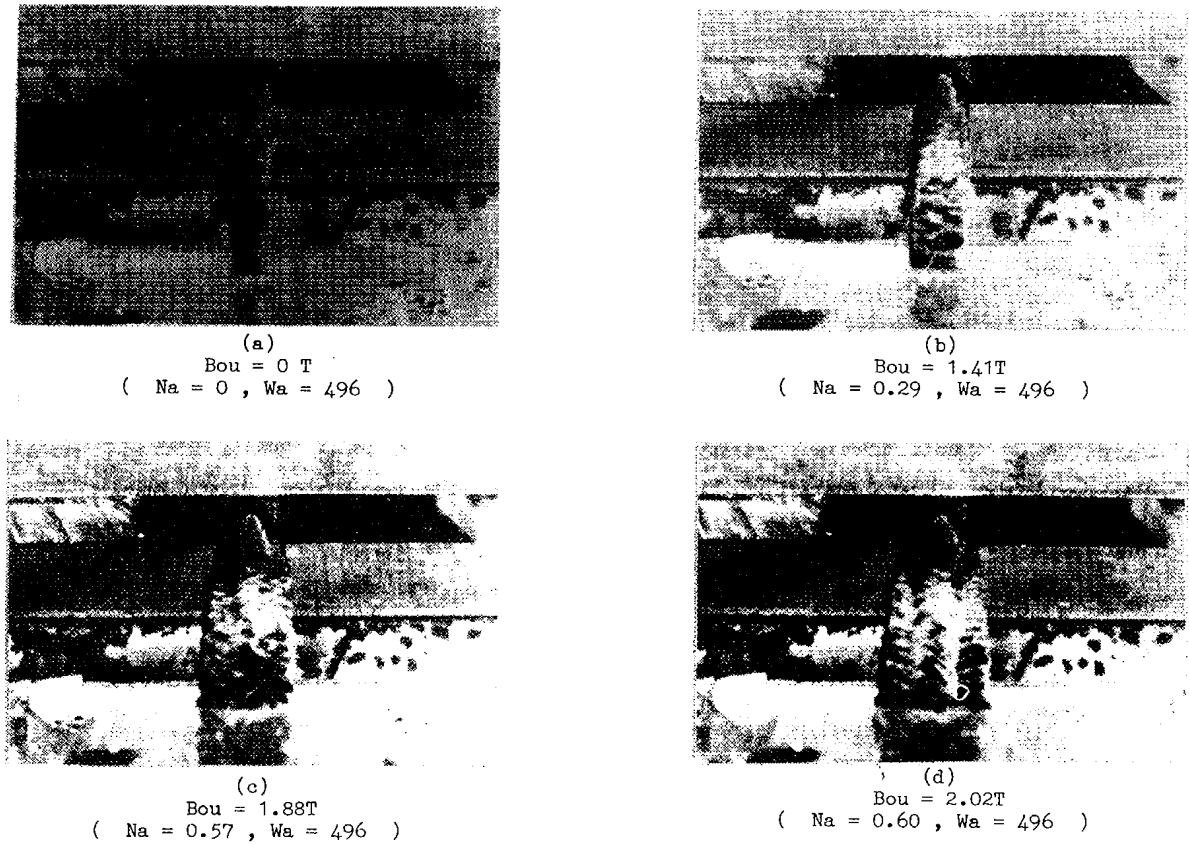


Fig. 9 Photographs of the jet for various applied magnetic field strengths

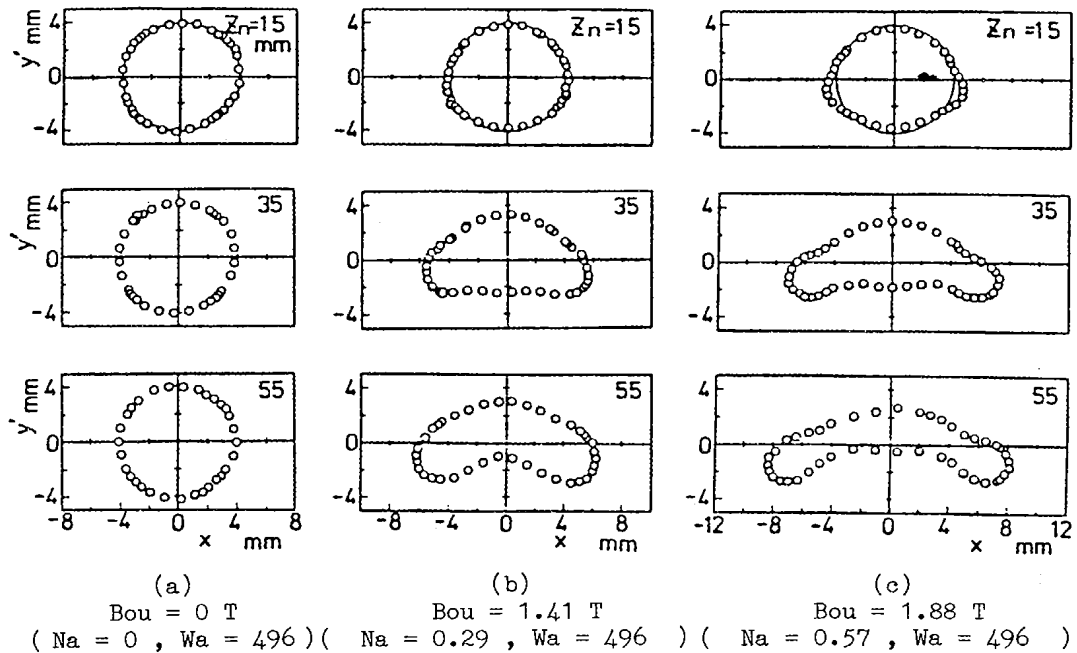


Fig. 10 Cross-sectional shape of the jet obtained by spot a electrode probe

increases with increasing applied magnetic field strength. In the case without a magnetic field, the jet shape remains almost circular at the origin. However, in the case with a magnetic field, the shape is different between the upper and lower halves. It may be considered that this asymmetry in shape is due to the non-uniformity of the exit velocity. In the process of the shape change, the fluid near the surface, where the axial velocity is small, is pushed to both sides, and then both sides hang down under the influence of gravity. The disturbances appear on the free surface of the jet, with or without an applied magnetic field.

The electromagnetic force has not only a lateral component but also a longitudinal component. Next, we examine the effect of the longitudinal force on the jet. The locus of the barycenter of the cross-sectional shape and the change in area are shown in Figs.11 and

12, respectively. The solid line in Fig.11 is the locus of the falling body with a horizontal velocity w_0 . The jet is changed in shape but not changed in area, and it describes almost the same parabola as a falling body. We conclude, from this, that the longitudinal electromagnetic force is smaller than the lateral one, and that the shape of the jet is changed mainly by the lateral force.

6. 2. 2 Dependence of the nozzle shape

We used two rectangular nozzles of almost the same cross-sectional area. We examined the effect of nozzle aspect ratio keeping w_0 and B_{0u} constant. The gap between the poles is 22mm. The photographs of the jet and the shapes obtained by measurements are shown in Figs.13 and 14 respectively. In the case without an applied magnetic field, the jet issuing from

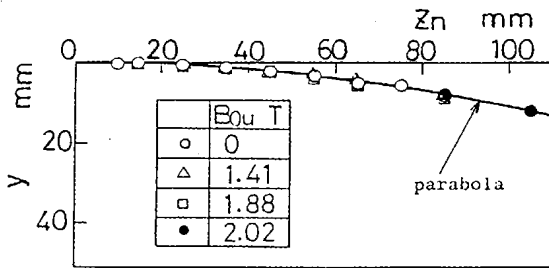


Fig. 11 Locus of the barycenter of the jet

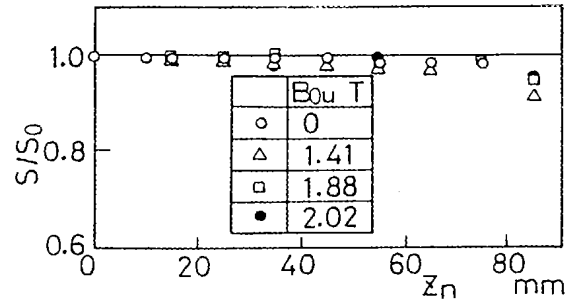
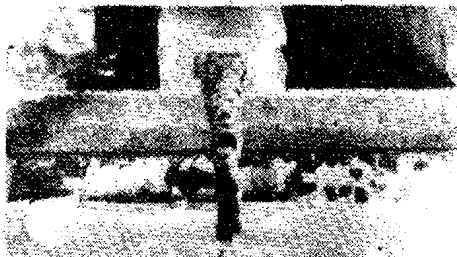


Fig. 12 Change in the jet area



$B_{0u} = 0$ T



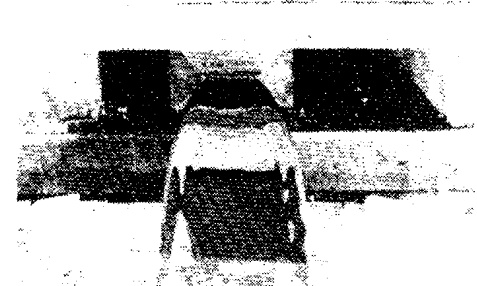
$B_{0u} = 1.97$ T

(a)

5 mm × 10 mm (bn/hn = 2)



$B_{0u} = 0$ T



$B_{0u} = 1.97$ T

(b)

3 mm × 15 mm (bn/hn = 5)

Fig. 13 Photographs of the jet issuing from a rectangular nozzle

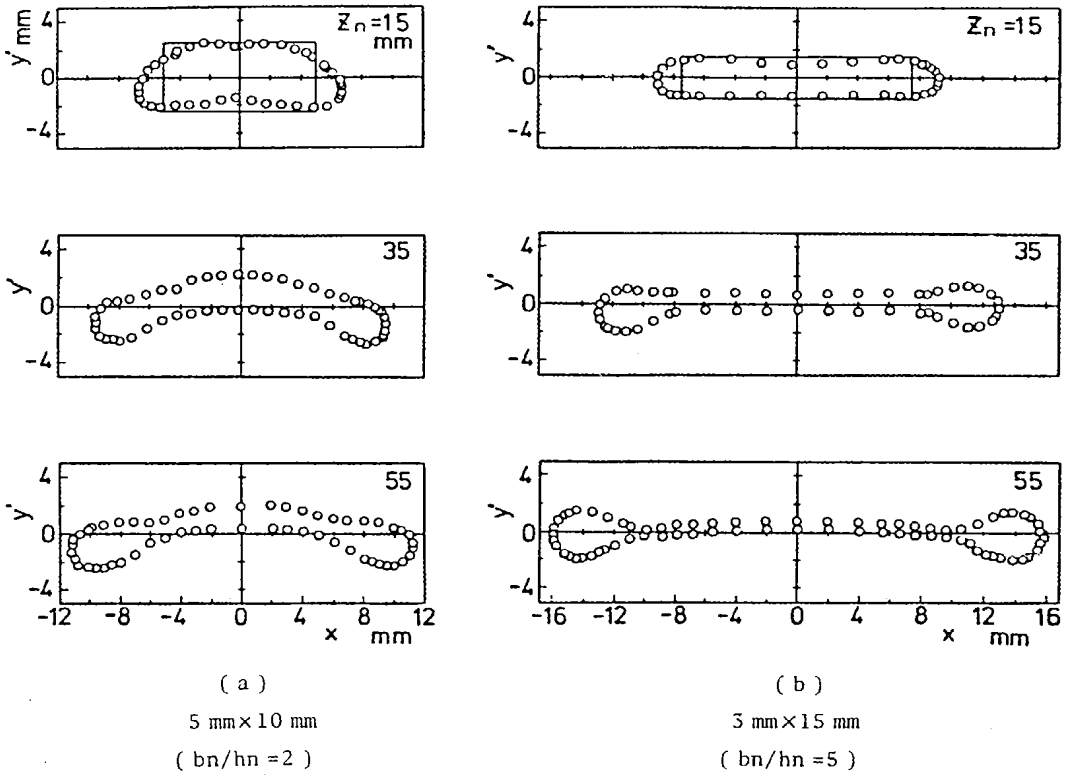


Fig. 14 Cross-sectional shape of the jet issuing from a rectangular nozzle

the rectangular nozzle, is longer along the width of nozzle which later on is changed to be longer in the vertical direction due to surface tension. On the other hand, in the case with an applied magnetic field, the jet is widened by the electromagnetic force. When the jet issues from a nozzle of large aspect ratio, the jet shape changed by the electromagnetic force is nearly symmetric along the y axis and almost uniform in thickness. Both sides of a jet issuing from a 3mm x 15mm rectangular nozzle become round with a change in shape, and they separate from the main part of the jet. We consider that surface tension and gravity have an important role in this separation, similar to the generation of a liquid drop. Fig. 15 shows the distribution of the jet aspect ratio b_j/h_j . In the case that the cross-sectional areas of the nozzles are same, the larger the nozzle aspect ratio b_n/h_n becomes, the greater the change in the jet aspect ratio b_j/h_j . The aspect ratio of the jet issuing from a rectangular nozzle of 3mm x 15mm increases up to 80 (see Fig.17).

6.3 Comparison of the jet shapes obtained experimentally and analytically

At first, we show the results for a liquid metal jet issuing from a rectangular nozzle without a magnetic field. When we calculate the jet shape, we use the modified Weber number as follows :

$$W'_a = \frac{\rho_l w_0^2}{\sigma} \sqrt{\frac{b_n h_n}{\pi}} \tag{76}$$

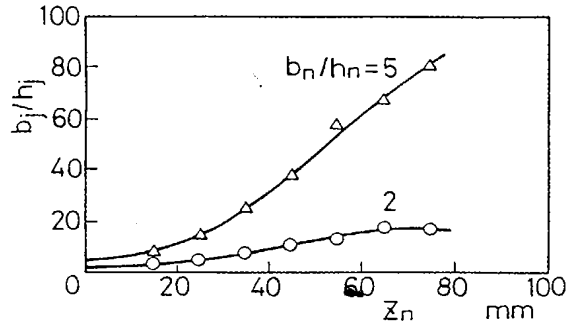


Fig. 15 Distribution of the jet aspect ratio

where b and h_n are the width and height of the rectangular nozzle, respectively. Fig.16 shows a comparison of the jet shapes obtained experimentally and analytically. We calculated the jet shape on the condition that $g^*_z = 0.33$ and $W'_a = 175$. The analytical results agree fairly well with the measurements and show well the oscillation of the jet shape due to surface tension.

Next, we show the results for a liquid metal jet under a non-uniform magnetic field. When we calculate the jet shape, we use the distribution of the applied magnetic field expressed by Eq.(67). Fig.17 shows a comparison of the jet widths obtained experimentally and analytically. We calculated the jet width under the condition that $W_a = 496$, $N_a = 0.29$ and $\epsilon_m = 0.645$. The analytical results agree fairly well with the

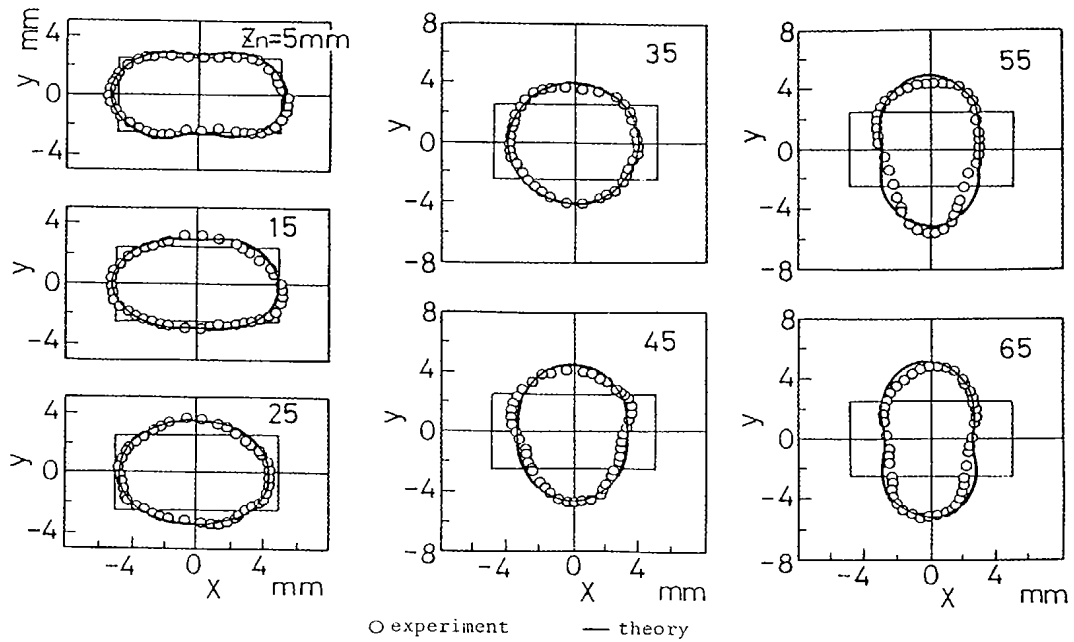


Fig. 16 Shape change of the jet issuing from a rectangular nozzle without a magnetic field

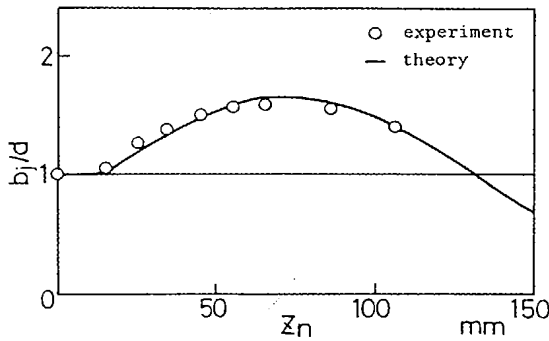


Fig. 17 Change in width of the jet issuing from a circular nozzle with a magnetic field

measurements and show well that the jet is widened by the electromagnetic force. Fig.18 shows the jet shapes. Though the measured shapes are asymmetric along the y axis under the influence of gravity, the calculated results agree qualitatively and explain well the effect of the electromagnetic force on the jet shape.

7. Conclusions

The shape of electrically conducting fluids under a non-uniform magnetic field was studied by an approximate analysis and by experiments with mercury, and the following results were obtained.

- (1) The magnetic field gradient changes the jet shape and acts on the jet like a wall, without coming into contact with the fluid.
- (2) Three parameters play important roles in the magnetic shape change, namely, the Stuart number

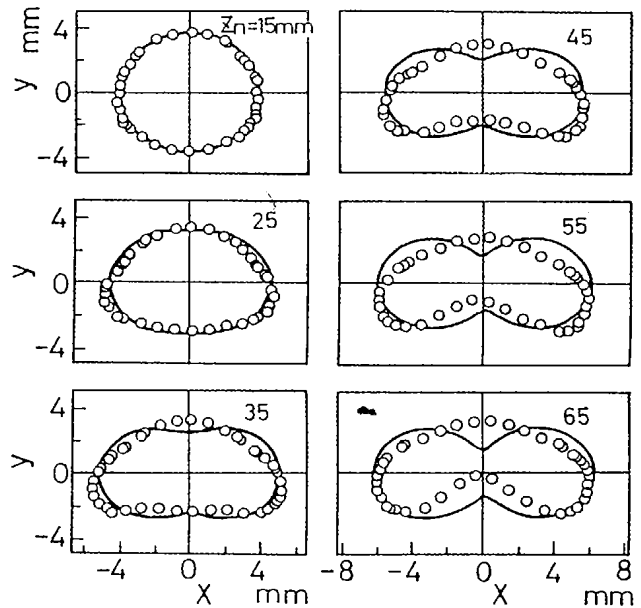


Fig. 18 Shape change of the jet issuing from a circular nozzle with a magnetic field

N_a , the Weber number W_a and the non-dimensional parameter ϵ_m .

- (i) In the case that W_a and ϵ_m are constant, the shape change increases with increasing N_a .
- (ii) In the case that N_a and ϵ_m are constant, the shape change increases with increasing W_a .
- (iii) The shape change tends to decrease with decreasing ϵ_m , but the effect of ϵ_m on the shape change is relatively small in comparison with the other parameters.

(4) A jet deformed by an electromagnetic force has almost the same area as the original jet.

(5) In the case that the cross-sectional area of a nozzle is constant, the larger the aspect ratio of the nozzle, the larger the change in the jet shape.

(6) A jet is widened under a negative magnetic field gradient, while a jet is changed in shape to be longer than it is wide under a positive one.

References

- (1) Shercliff, J. A., Proc. R. Soc. London, Ser. A., Vol. 375 (1981), 455.
- (2) Etay, J. and Garnier, M., Proc. Symp. Int. Union of Theoretical and Applied Mech., (1982), 190.
- (3) Garnier, M., Prog. Astro. Aero., Vol. 84 (1983), 433.
- (4) Oshima, S., Yamane, R., Mochimaru, Y. and Sudou, K., Bull. Jpn. Soc. Mech. Eng., Vol. 29, No. 253 (1986-7), 2070.
- (5) Oshima, S., Yamane, R., Mochimaru, Y. and Sudou, K., Bull. Jpn. Soc. Mech. Eng., Vol. 29, No. 253 (1986-7), 2070.
- (6) Rayleigh, L., Proc. R. Soc., Vol. 29, No. 196 (1879), 71.
- (7) Weber, C., Z. Angew. Math. Mech., Vol. 11 (1931), 136.
- (8) Taylor, G., Proc. R. Soc. London, Ser. A, Vol. 259, No. 1296 (1960), 1.
- (9) Clarke, N. S., J. Fluid Mech., Vol. 31, No. 3 (1968), 481.
- (10) Longuet-Higgins, M. S., J. Fluid Mech., Vol. 55, No. 3 (1972), 529.
- (11) Tuch, E. O., J. Fluid Mech., Vol. 76, No. 4 (1976), 625.
- (12) Green, A. E., Acta. Mech., Vol. 26 (1977), 171.
- (13) Geer, J. F., Phys. Fluid, Vol. 20, No. 10 (1977), 1613.